ASM Sc. J., 20(2), 2025
https://doi.org/10.32802/asmscj.2025.1662

Removal of Chloramphenicol Compounds Using Coconut Husk-Based Adsorbent

N. A Hamid* and L.S. Azmi

School of Chemical Engineering, Engineering Campus, Universiti Sains Malaysia, 14300 Nibong Tebal, Penang, Malaysia

The improper treatment of Chloramphenicol (CAP) compounds prior to its discharge has become a serious issue, as the buildup of CAP may become a serious threat to public and aquatic lives. This study suggests the utilisation of coconut husk-derived activated carbon (CHAC) prepared via hydrothermal carbonisation (HTC) at 220˚C for 2 hours prior to $ZnCl_2$ activation for the effective removal of CAP compounds from a water mixture. The efficiency of the prepared CHAC was evaluated at diverse parameters such as solution pH ranging from 3 to 11 and initial concentrations of CAP solution of 100 mg/L to 400 mg/L, in which results show the highest CAP removal of 99.99% at 200 mg/L with an optimum pH of 9. The remarkable CHAC performance on CAP removal matches with the surface area as well as pore volume of 740.7451 m^2/g and 0.2476 cm^3/g, correspondingly. Moreover, the adsorption of CHAC onto CAP was governed by chemisorption as suggested by Pseudo-second order. The findings acquired from this study strongly suggest that CHAC has excellent adsorption performance and properties, and it is also economically feasible due to high adsorption capacity and environmentally friendly.

Keywords: adsorption; characterisation; hydrothermal carbonisation; chloramphenicol compound; coconut husk

I. INTRODUCTION

The excessive use of chloramphenicol (CAP) and improper post-treatments prior to its effluent discharge has become very concerning as the build-up of the residual CAP industrial water effluents will eventually cause their carcinogenicity, mutagenicity, toxicity, and other ecological parameters becomes more significant and worrying (National Centre for Biotechnology Information, 2021). Chloramphenicol (CAP) is an antibiotic especially in the pharmaceutical industry as a main ingredient for eye ointments and ear drops, also for making mouthwashes, toothpastes, moisturisers and others (Feder *et al*., 1981). Extensive use of this emergent antibiotic pollutant in various sectors including aquaculture and human leads to the massive pollution in water sources such as river, lake and others (Lach J, 2019; Nguyen *et al*, 2022). To solve this issue, the removal of CAP from wastewater is crucial to avoid the consequential risks that may arise from the build-up of this chemical. The use of biomass-derived activated carbons (ACs) as adsorbent for antibiotics residuals in wastewater has been identified to be a promising alternative as it also contributes to the sustainability of the environment (Bello *et al*., 2020; Chen *et al.,* 2021). Coconut husks are a natural byproduct of coconut farming, which is a renewable resource. As coconuts are harvested regularly, and their husks are typically discarded as waste, thus by converting these husks into activated carbon is considered to be sustainable. Coconut husk is a lignocellulosic biomass that is widely available, cheap, and biodegradable. It is a part of a coconut that is made up of about 60% cellulose and lignin (Man *et al*., 2015; Foo & Hameed, 2012; Liew & Hamid, 2023). In Malaysia, approximately 6,000 to 10,000 nuts per hectare are produced each year, whereas nearly 10 million hectares of nuts are produced worldwide by 92 different countries, with 75% of the production is contributed by Asian countries (Ahmad *et al*., 2021). The growing demand of

*Corresponding author's e-mail: chrina@usm.my

coconuts husk has greatly increased ever since 10-20 years ago, with 100-220 million coconut fruits being imported worldwide each year, especially during festive seasons (Yun, 2019). The use of coconut husk as an AC allows the conversion of agricultural wastes into useful applications and reduce land as well as water pollutions. Although many studies have utilised different types of biomasses such as rice husk and empty oil palm fruit bunches in the manufacture of AC, coconut husk has been one of the most preferred options as it has numerous favourable characteristics, including high carbon content, great strength, lower ash content and high volatile content (Man *et al.*, 2015).

The preparation of the coconut husk-derived AC via HTC, followed by chemical activation of hydrochar have been widely utilised by a lot of researchers due to lower operating conditions and excellent AC properties. Many research studies have presented the productivities of other biomass-derived activated carbon with $ZnCl_2$ activation such as coconut shell, *salacca* peels, soybean dregs and bitter kola nut shells (Islam *et al.,* 2017; Jain *et al.,* 2015; Kristianto *et al.,* 2020; Li *et al.,* 2020; Idris-Hermann *et al.*, 2018). Previously, mesoporous activated carbon prepared via a hydrochar derived from coconut shell waste through hydrothermal carbonisation and NaOH chemical activation process shows maximum adsorption capacity of 200.01 mg/g (Islam *et al.,* 2017). Jain *et al.* (2015) prepared coconut shell-derived AC via $ZnCl_2$ activation and the recorded a q_{max} of 264 mg/g for the adsorption of phenol compounds. On the other hand, Kristianto *et al.* (2020) reported a bagasse-derived AC prepared via $ZnCl_2$ activation and the produced q_{max} for the adsorption of Cr(VI) was 88.88 mg/g. Meanwhile, Li *et al.* (2020) and Idris-Hermann *et al.* (2018) reported a similar synthesis condition for the preparation of soybean dregs- and bitter kola nut shells-derived ACs, in which both samples give the highest achievable q_{max} by soybean dregs-derived AC and bitter kola nut shells-derived AC for dye removals are 255.10 mg/g. and 72.59 mg/g, respectively. On the flip slide, guava seed-derived AC provides q_{max} of 80.50 mg/g for green dye removal. Anyhow, the study on the production of coconut husk-derived activated carbon with $ZnCl_2$ activation is still lacks in investigation for comparative analysis. Hence, the objective of this study is to observe the efficiency of coconut husk-derived activated carbon with $ZnCl_2$ activation by evaluating its physicochemical properties and adsorption performance on the removal of CAP compounds.

II. MATERIALS AND METHOD

The coconut husk, which is the raw material for the experiment is obtained locally around Nibong Tebal, Penang and was labelled as raw coconut husk (RCH). The coconut husk was rinsed with distilled water prior to drying at 120˚C for 5 hours. Then, this raw coconut husk grounded into small particles using a grinder. To ensure uniform sizes of particles, the crushed particles were sieved into 10-20 mesh sizes. The hydrothermal carbonisation (HTC) of the prepared coconut husk samples was done in a 200 mL stainless-steel reactor. A 5 g of the coconut husk and 150 mL of distilled water were mixed and placed in the reactor, and the treatment is conducted at a fixed HTC temperature of 220˚C for 2 hours (Islam *et al.,* 2017). Then, the reactor was set to lower the temperature before the hydrochar was taken out and filtered using a filter paper. The hydrochar obtained was then thoroughly washed using distilled water twice to remove water-soluble volatile matters and then dried at 120˚C over the night before it is chemically impregnated with $ZnCl_2$. The yield of hydrochar was determined using Equation 1:

$$Hydrochar\ yield\ (\%) = \frac{W_{char}}{W_{ch}} \times 100\% \qquad (1)$$

where W_{char} and W_{ch} are the weight of hydrochar and coconut husk, respectively.

Hydrochar were then mixed with $ZnCl_2$ solution in appropriate quantities to ensure the desired '$ZnCl_2$:husk' ratio of 3:1 is achieved. After mixing, the hydrochar was recovered and desiccated in the muffle oven at 120˚C for 5 hours (Islam *et al.,* 2017). After drying, the dried hydrochar was subjected to the microwave irradiation activation method. Approximately 2 g of dried hydrochar was mounted inside a Pyrex glass tube prior loading inside the microwave's chamber. The microwave was run at fixed radiation power of 515 W for 6 minutes. During this step, CO_2 gas was allowed to flow through the chamber at a flow rate of 150 cm^3/min to give a gasification impact on the sample. After activation, the resulting AC produced was collected and labelled as coconut husk activated carbon (CHAC). The yield of CHAC was determined using the formula as in Equation 2:

$$CHAC\ yield\ (\%) = \frac{W_f}{W_i} \times 100\% \quad (2)$$

where W_f and W_i are the weight of CHAC and dried coconut husk, respectively.

A. Chemical and Physical Characterisation

1. Brunauer–Emmett–Teller (BET) analysis

BET (Micromeritics ASAP, 2020) were employed to determine the surface areas and pore volumes of CHAC and RCH. About 0.5 g of CHAC and RCH samples were prepared and degassed for 12 hours at 120˚C.

2. Scanning Electron Microscopy (SEM) analysis

SEM modelled FEI Quanta 450 was used to identify the morphologies of CHAC and RCH. The observations on the surface morphologies of CHAC and RCH samples were done at four (4) various intensifications which is 500x, 1000x, 3000x and 5000x.

3. Fourier Transform Infrared (FTIR) Spectroscopy analysis

Fourier Transform Infrared (FTIR) Spectroscopy (IR prestige 21) was used to determine the existing functional groups that are present within the molecules of CHAC and RCH.

B. Adsorption of Chloramphenicol Compound (CAP)

1. Preparation of CAP solution

Chloramphenicol (CAP, purity of > 98%) was purchased from Aladdin (Shanghai, China). 1 L of various CAP stock solutions ranging from 100 mg/L to 400 mg/L with 100mg/L interval were prepared by mixing 0.1 g to 0.4 g of CAP powder with 1 L of distilled water, individually. Each solution was mixed at 30˚C for 1 hour to obtain equilibrium prior to adsorption experiments.

2. Batch adsorption of CAP

Batch adsorption was performed in 250 mL conical flasks, comprising a mixture between 0.1 g of CHAC and 100 mL of CAP solution whilst the absorbance values were measured using UV-vis spectrophotometer (UV-1800, Shimadzu) with 400 nm wavelength. The capacity of adsorption and efficiency of CAP removal were ascertained using Equation (3) and (4):

$$Adsorption\ capacity, Q_e = \frac{(C_0 - C_e)V}{W} \quad (3)$$

$$Removal\ efficiency\ (\%) = \frac{C_0 - C_e}{C_0}\ x\ 100 \quad (4)$$

where;

Q_e = capacity of adsorption (mg/g)

C_o = concentration of CAP solution at initial (mg/L)

C_e = equilibrium concentration of CAP solution (mg/L)

V = volume of solution (L)

W = mass of adsorbent (g)

3. Adsorption at different pH of CAP solution

The capacity of CHAC adsorption was investigated at different pH of CAP solution by adding either 0.1 M HCl or NaOH solution. In this experiment, the pH of CAP solution was adjusted at 3, 5, 7, 9 and 11, with a fixed CAP concentration of 200 mg/L. 0.1 g of CHAC was added to each flask containing 100 mL of CAP solution of different pH. The mixture was agitated at 25˚C in a thermostatic shaker bath for 3 h at a stirring speed of 100 rpm to ensure adsorption equilibrium. The optimum pH was then determined and fixed for the next parameter study.

4. Adsorption at different initial concentrations of CAP solution

The adsorption capacity of CHAC was observed at different initial CAP concentrations from 100 mg/L to 400 mg/L at optimum pH which was determined earlier. The mixture was agitated at 25˚C in a thermostatic shaker bath for 3 h at a stirring speed of 100 rpm to ensure adsorption equilibrium. Similarly, a small amount of sample (approximately 4.5 mL) was taken out of each flask using a nylon syringe filter (0.45 μm) at different contact time intervals during the experiment to determine the concentration of CAP solution at the respective contact time.

5. Isotherms of Adsorption

The isotherm of adsorption was conducted to gain information on the mobility or retention of adsorbate on the surface of the adsorbent. The isotherm of adsorption correlates the equilibrium data from the experiment to further assist the understanding of the adsorption system.

6. *Langmuir isotherm*

Langmuir isotherm model suggests that the adsorption take place on a finite number of surface sites of the adsorbent through monolayer adsorption with no movement of adsorbate in the surface plane (Tan *et al.,* 2008). Briefly, the Langmuir isotherm assumes that a monolayer (single layer) is formed when adsorbate adheres on the surface site of an adsorbent without involving any interaction between the absorbed particles, and maximum adsorption is achieved when the surface of the adsorbent is completed covered by the monolayer of adsorbed particles (Hammond & Corner, 2013). The non-linear form of Langmuir isotherm is given by Equation 5:

$$q_e = \frac{q_0 K_L C_e}{1 + K_L C_e} \quad (5)$$

Upon linearisation, the Langmuir isotherm can be simplified to:

$$\frac{C_e}{q_e} = \frac{1}{q_0 K_L} + \frac{C_e}{q_0} \quad (6)$$

where;

q_e = amount of CAP adsorbed at equilibrium (mg/g)

q_o = saturated monolayer sorption capacity (mg/g)

K_L = Langmuir isotherm constant (L/mg)

C_e = concentration of adsorbate at equilibrium (mg/L)

From the equation, the values of q_o and K_L can simply be obtained from the plot of C_e/q_e vs C_e.

7. *Freundlich isotherm*

Freundlich isotherm model explains the more than one layer and non-ideal adsorption process that occurs on heterogeneous surface of adsorbent via empirical equation (Freundlich, 1906). The isotherm model is generally derived by presumptuous that both cations and anions of adsorbate are adsorbed onto the same external layer of adsorbent simultaneously (Nakahara, 1996). The non-linear form of Freundlich is given by Equation 7:

$$ln\ q_e = \ln K_F + \frac{1}{n} \ln C_e \quad (7)$$

in which;

q_e = quantity of CAP adsorbed at equilibrium (mg/g)

K_F = Freundlich isotherm constant ((mg/g).(L/mg)$^{1/n}$)

n = adsorption strength

C_e = concentration of adsorbate at equilibrium (mg/L)

Thus, the quantities of n and K_F can simply attained from the plot of ln q_e vs ln C_e.

8. *Adsorption kinetics*

The adsorption kinetic study was done to clarify the controlling stage of the adsorption process, alongside the mechanism of adsorption of CAP particles onto CHAC. It generally describes the extent of adsorption with respect to time and is used to determine the diffusion of adsorbate onto the adsorbent surface. In this study, two kinetic models, namely the pseudo first order kinetic model and pseudo second order kinetic model are used to validate the dynamic figures obtained from the experiment.

9. *Pseudo first order kinetic model*

This kinetic model describes an adsorption process through the diffusion of particles across a boundary. Lagergren kinetic equation (Equation 8) shows pseudo first order kinetic model (Kowanga *et al.*, 2016).

$$\frac{dq}{dt} = k_1(q_e - q) \quad (8)$$

Upon integration, the Lagergren kinetic equation further derived to obtain the non-linear and linear equations as shown in Equation 9 and 10:

$$q_t = q_e(1 - e^{-k_1 t}) \quad (9)$$

$$\ln(q_e - q_t) = \ln q_t - \frac{k_1}{2.303} t \quad (10)$$

in which;

q_e = quantity of CAP adsorbed at equilibrium (mg/g)

q_t = quantity of CAP adsorbed at time, t (mg/g)

k_1 = rate constant for first order kinetics (min^{-1})

t = contact time (min)

From the equation, the value of k_1 can simply be obtained from the draw of ln (q_e - q_t) vs t.

10. *Pseudo second order kinetic model*

The pseudo second order kinetic model is generally utilised to estimate the behaviour of the adsorption process. This kinetic model is often used with chemisorption as the rate-controlling step (Kowanga *et al.*, 2016). Upon integration, the pseudo second order kinetic model above further derived to

yield the non-linear and linear equations as in Equation 11 and 12:

$$q_e = \frac{k_2 {q_e}^2 t}{1 + k_2 q_e t} \quad (11)$$

$$\frac{t}{q_t} = \frac{1}{k_2 {q_e}^2} + \frac{1}{q_e} t \quad (12)$$

where;

q_e = amount of CAP adsorbed at equilibrium (mg/g)

q_t = amount of CAP adsorbed at time, t (mg/g)

k_2 = rate constant for second order kinetics (g/mg.min)

t = contact time (min)

From the equation, the values of q_e and k_2 can simply be obtained from the plot of t/q_t vs t.

III. RESULT AND DISCUSSION

A. Characterisation of CHAC

1. BET analysis

Table 1 shows that significant improvement on coconut husk-derived activated carbon (CHAC) was observed, where the pore surface area has increased from 22.953 m^2/g to 740.645 m^2/g as compared to raw coconut husk (RCH).

Table 1. Porosity structure of CHAC

Sample	BET surface area (m^2/g)	t-Plot external surface area (m^2/g)	t-Plot micropore area (m^2/g)	Lang-muir surface area (m^2/g)	Pore volume (cm^3/g)
RCH	22.953	29.757	NA	38.729	-0.004
CHAC	740.745	239.736	501.009	1029.169	0.248

Such improvement in the surface area obtained after the chemical activation indicates a much better platform for adsorption. As the surface area increases, more adsorbates can be captured or adsorbed onto the surface of CHAC. The result explained also corresponds to the development of pore volume and Langmuir surface area of 0.248 cm^3/g and 1029.169 m^2/g, respectively. Apparently, the integration of chemical activation of coconut husk-derived hydrochar using $ZnCl_2$ with microwave irradiation technique has successfully upgraded the structures of activated carbons, making it more suitable for removal experiments. This is attributed to the swelling effects caused by the breaking of lateral bonds between the cellulose molecules of the sample which is assisted by $ZnCl_2$. Thereby, more inter- and intra-granular voids which is 0.248 cm^3/g of pore volume are formed which leads to the development of the microporosity (Allwar *et al.*, 2008). Previously, Yusop *et al.* (2021) reported that the gasification of CO_2 gas onto the coconut husk samples enable deep penetration of CO_2 gas into the core surface of coconut husk, thus promoting the development of pores.

2. Scanning Electron Microscopy Analysis

Figure 1 and 2 (a-d) depicts the SEM micrographs of RCH and CHAC at different magnifications, respectively. Overall, there is a huge observable morphology difference between RCH and CHAC. As presented on Figure 1(a), there are barely available pores for adsorption observed on the surface of sample, which explains the lower surface area observed RCH in BET analysis. In addition to the lower pore availability for adsorption, the surface of RCH also seemingly rough and uneven. Apparently, with higher magnifications, as seen on Figure 1(b), (c) and (d), the in-depth pore structure becomes more visible for comparison, whereby it is observable that the pore openings of irregular shapes are apparently pointing out in various directions.

The SEM micrographs for CHAC presented in Figure 2, apparently shows a better morphology that that of RCH. From Figure 2(a) and (b), the pore distributions of CHAC are more consistent, along with increasing availability for adsorption. In comparison with RCH, the porosity of CHAC seems to have developed incredibly, in which cavities are observable at every side of the CHAC surface. In addition, as seen on Figure 2(c) and (d), the pores shapes of CHAC are spherical shapes with better distributions than those observed for RCH. Such observable improvement in porosity

post-activation can be attributed to the breakdown of lignocellulosic components of CHAC with increasing temperature (Ajala *et al.,* 2023).

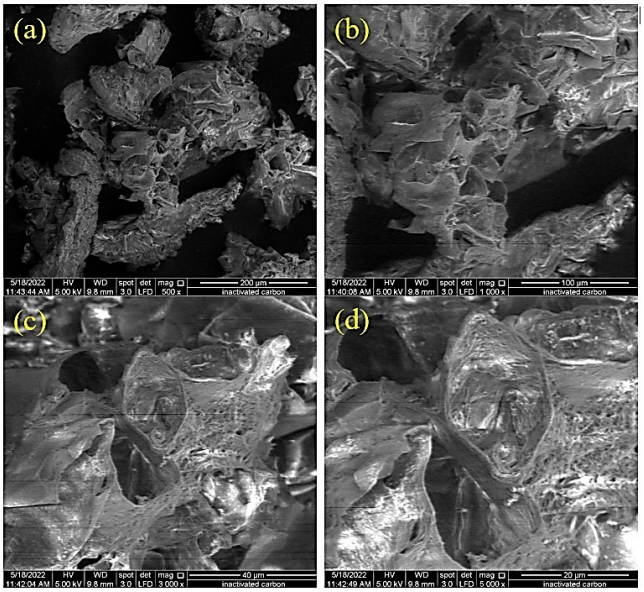

Figure 1. SEM micrographs of RCH at magnifications of (a) 500, (b) 1000, (c) 3000 and (d) 5000.

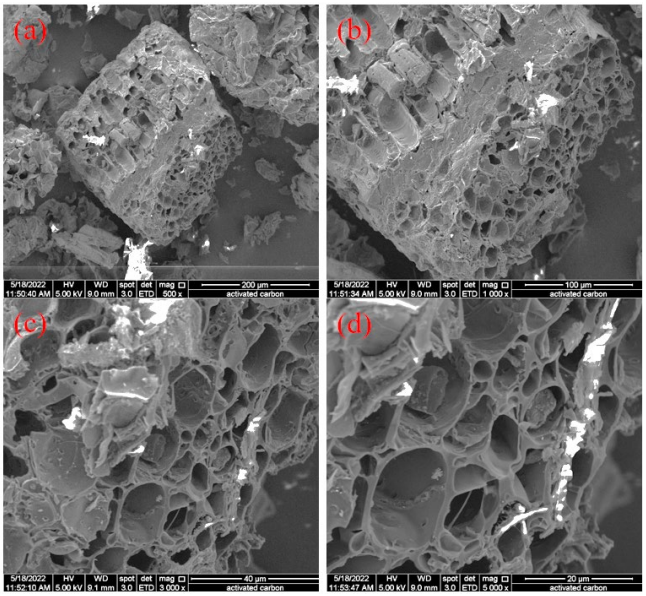

Figure 2. SEM micrographs of CHAC at magnifications of (a) 500, (b) 1000, (c) 3000, and (d) 5000.

4. *FTIR Analysis*

Figure 3 illustrated FTIR spectrum of CHAC. Medium peak absorption bands at 3842.2 cm^{-1} and 3707.18 cm^{-1}, where both peaks correspond to O-H stretching of alcoholic compound in line with earlier work reported by Bello *et al.* (2020) which also used coconut husk activated carbon. A similar but stronger and broader intensity band is observed at 3408.22 cm^{-1} which also attributes to the O-H bonds stretching. According to Sultana *et al.* (2022), the observable peaks at the bands mentioned denote the existence of cellulose and lignin on the surface of CHAC. A weak peak observed at 2331.94 cm^{-1} attributes to the presence of C≡C bond, whereas the weak peak at 1544.63 cm^{-1} implies the existence of cyclic alkene or C=C bond. Lastly, the strong and broad peak observed at 1035.77 indicates the elongating vibration of C-O bond and the presence of an alkyl aryl ether on CHAC. It is also noted that O-H stretching vibrations are also observed at bands of 3778.55 cm^{-1} and 3452.58 cm^{-1} (Bello *et al.*, 2020). Meanwhile, incidence of C≡C bond is recorded at absorption band of 2331.94 cm^{-1}.

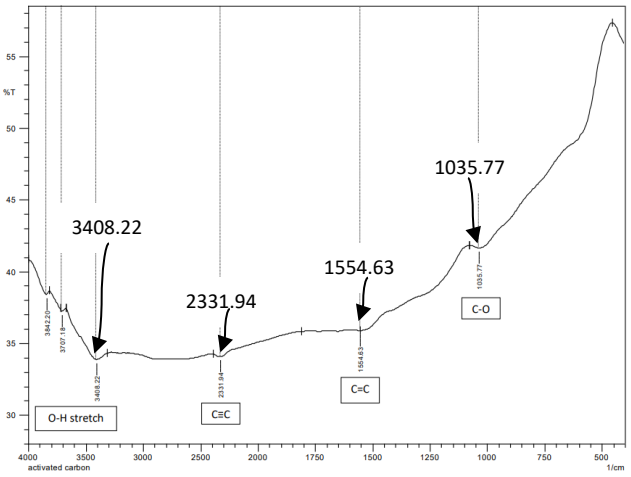

Figure 3. FTIR spectrum of CHAC

5. *Hydrochar and activated carbon yield*

The overall amount of hydrochar yield obtained from this study via HTC at 220˚C and 2 h carbonisation is 81.16%. It is apparent that the hydrochar yield obtained from this experiment is much higher than using olive pomace, Eucalyptus bark, and coffee husk at the same temperature. Yay *et al.* (2021) presented a maximum of 70.24% yield for olive pomace hydrochar prepared via HTC method at 220˚C. On the other hand, Sharma *et al.* (2020) reported a much lower yield, in which the maximum yield reported for Eucalyptus bark-derived hydrochar was only 46.4%. Meanwhile, Hien *et al.* (2016) reported a yield of 50.2% for coffee husk-derived hydrochar. Nonetheless, the drops in hydrochar yield as observed from studies mentioned earlier

proved that the type of biomass waste used plays significant role in determining the yield although similar carbonisation temperature of 220˚C applied during preparation of hydrochars. Each of lignocellulosic biomass contains different amount of cellulose, hemicellulose and lignin and these will greatly influence the yield of hydrochars. For example, the overall yield presented by Yay *et al.* (2021) is based on the carbonisation period of 1 hour, whereas the yield presented by Hien *et al.* (2016) was based on the carbonisation period of 6 hours, except for Sharma *et al.* (2020) in which the yield presented were based on the same conditions as this work. Besides carbonisation period, the difference in hydrochar yield is also affected by the HTC temperature, in which Hien *et al.* (2016) suggested that the drop in hydrochar yield is due to the hydrolysis, carboxyl reduction, aromatase and polymerisation reactions that occur at higher temperature. However, the yield of hydrochar obtained from this study is still much higher than those of olive pomace, Eucalyptus bark, and coffee husk-derived hydrochar which produced at the same temperature. Thereby, this suggests the potential of coconut husk-derived hydrochar as an adsorbent as it is capable to produce a higher yield at 200˚C.

On the other hand, the overall yield of CHAC obtained from $ZnCl_2$ activation and CO_2 gasification method has resulted in a maximum yield of 83.84%. The CHAC yield resulted from KOH activation and CO_2 gasification suggested by Tan *et al.* (2008) at 816˚C and 811˚C activation temperatures were 15.50% and 19.20%, respectively. The huge difference observed suggests the effectiveness of chemical activation of coconut husk using $ZnCl_2$ compared to that of KOH. It was observed that the highest amount of activated carbon was recorded with 'KOH:coconut' husk ratio, activation period and temperature of 3.9, 816˚C and 1 hour, respectively. Highest CHAC yield is obtainable with increase in chemical impregnation ratio, as higher ratio promotes catalytic oxidation leading to improvement of pore development of the CHAC (Sharma *et al.*, 2020). Also, higher activation temperature will promote gasification of the carbon, which will in turn improve the porosity of the sample. On the other hand, increasing activation time will provide ample reaction rate for the pore development. It denotes that CHAC preparation with $ZnCl_2$ activation is another alternative that worths a wider implementation for adsorption studies.

B. Adsorption Performance

1. Effect of solution pH

Figure 4 depicts an increase in CAP removal is observed with increasing pH with maximum of 99.95% at pH 9. Whereas almost similar CAP removal recorded at lower pH indicating this reaction is favourable in alkaline based condition. This finding can be explained based on the surface properties of negatively charged CHAC. In general, the CAP particles, which are cationic, will naturally bind to the negatively charged surface of CHAC as electrostatic pulls among the adsorbent and adsorbate. At lower pH of solution, the H^+ ions concentration in the solution will build up and eventually create a competition with the cationic CAP particles for a binding site. This phenomenon consequently results in a greater electrostatic repulsion on the CHAC surface. Hence, the CAP particles uptake will become less efficient, leading to poorer removal efficiency and lower adsorption capacity.

The results obtained in line with the results reported by Yu *et al.* (2019) that the highest CAP removal is obtained at pH of 9, which agrees with the result obtained from this experiment. This report also justified that the decrease in CAP removal at lower pH is due to the increasing concentration of H^+ ions, which interferes with the adsorption of CAP on the adsorbent surface. On the other hand, the results presented by Zhang *et al.* (2021) also agrees that the highest CAP removal is achieved at higher pH value. In this study, the CAP removal is the lowest at pH of 1, and then gradually increases with increasing pH. The highest CAP removal is attained at pH of 10.36, but the removal efficiency slowly declines as the pH is further increased to 12 (Zhang *et al.*, 2021). The efficiency of CHAC on another experiment can also be compared with the results obtained from this study, where the lowest crystal violet (CV) removals using CHAC presented by Sultana *et al.* (2022) are observed at lower pH from 1 to 4, due to the stronger repulsion between the CHAC and the cationic dye particles. As the solution pH increases to 5, the adsorption capacity noticeably increases to a maximum dye removal of 82%, and then slowly declined as the pH is further increased from 6 to 12.

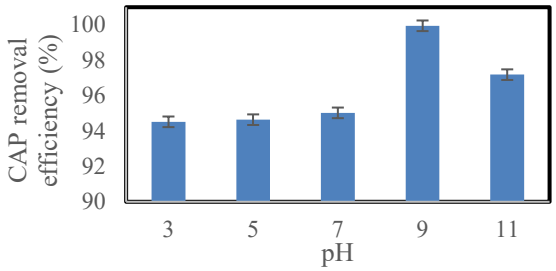

Figure 4. CAP removal efficiency (%) at different pH of solution.

2. Effect of Initial Concentration

Figure 5 shows adsorption capacities for all different concentrations increase over time and slowly settles at equilibrium after 50 minutes. During the first 20 minutes of the experiment, the adsorption capacity for all concentrations surges significantly, owing to the massive number of available surface sites that were accessible for CAP uptake. However, it is noticeable that longer time is taken to reach equilibrium as the concentration rises to 400 mg/L from 100 mg/L. After just 30 minutes, the uptake of CAP solution at 100 mg/L solution slowly becomes steady and reaches equilibrium until the end of the experiment. Here, the equilibrium at 100 mg/L is achieved with highest adsorption capacity of 100.393 mg/g. However, it was observed that for 200 mg/L, 300 mg/L and 400 mg/L concentration requires 75, 150 and 90 minutes, respectively to reach equilibrium. These results correspond to the maximum adsorption capacities of 200.901 mg/g, 270.985 mg/g and 261.165 mg/g for CAP concentrations of 200 mg/L, 300 mg/L and 400 mg/L, correspondingly.

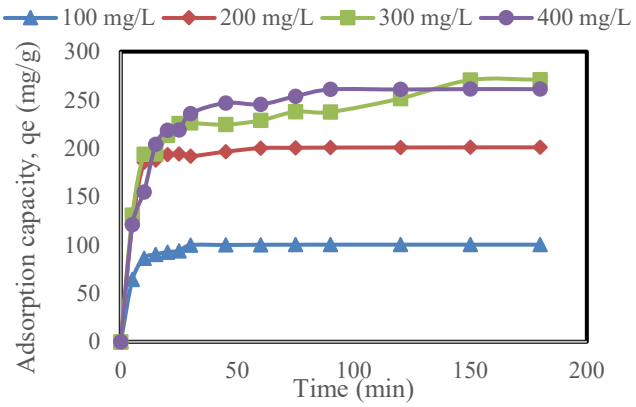

Figure 5. Effect of initial concentration on CAP removal using CHAC.

The removal efficiency of CAP declines from 99.99% to 99.95%, 90.03% and 65.08% at CAP concentrations of 100 mg/L to 400 mg/L, respectively. From the finding, it seems that the interactions between the surface sites of CHAC and CAP particles are more efficient at lower concentrations than higher concentrations. This is because, more CAP is impregnated on the CHAC surface at higher concentrations, which eventually retard the ability of the AC to adsorb further (Yu *et al.*, 2019). Thus, this explains the drop in CAP removal ability with increasing concentration.

3. Adsorption Isotherm and Kinetics

Figure 6 depicts the non-linear graph of Langmuir and Freundlich isotherm models compared to the experimental data from this study. As seen on Figure 6, the curve trend of the Langmuir isotherm data follows closely to the curve trend of experimental data from this study. The Freundlich isotherm non-linear data, however, did not show any representation with the varying CAP concentration. In addition, the highest adsorption capacity, q_m obtained from the Langmuir isotherm model (263.158 mg/g) is close to the highest capacity of adsorption, q_e obtained from the experiment (261.165 mg/g). On the other hand, Freundlich isotherm provides highest adsorption capacity of 187.073 mg/g which is far from the experimental data. Also, the Langmuir isotherm model was calculated to have a correlation efficient (R^2) value of 0.9999, which is higher than the Freundlich isotherm model (R^2 = 0.7671).

To further validate the model accuracy, the calculated data for both Langmuir and Freundlich isotherms are further analysed by determining the root mean squared errors (RMSE) for each model, respectively. Generally, lower RMSE is more preferrable as it indicates a better model accuracy and performance. The RMSE value obtained for Langmuir isotherm model is 8.0264, which is lower than the RMSE of the Freundlich isotherm model (RMSE = 32.9469). Hence, this further justifies that the adsorption of CAP using CHAC from this experiment is best described by the Langmuir isotherm model.

Now, it can be strongly justified that the adsorption process in this study occurs on the homogeneous surface of the adsorbent, with no interactions between the adsorbed particles involved. This analysis agrees with the report

presented by Zhang *et al.* (2021), where the adsorption of CAP is best described using the Langmuir isotherm model. Based on the report, the Langmuir isotherm model accuracy at room temperature is confirmed with R^2 value of 0.987, which is higher than the Freundlich and Temkin isotherm models with R^2 value of 0.868 and 0.959, respectively.

This shows that the Langmuir isotherm model provides higher accuracy than that of Freundlich model for this study.

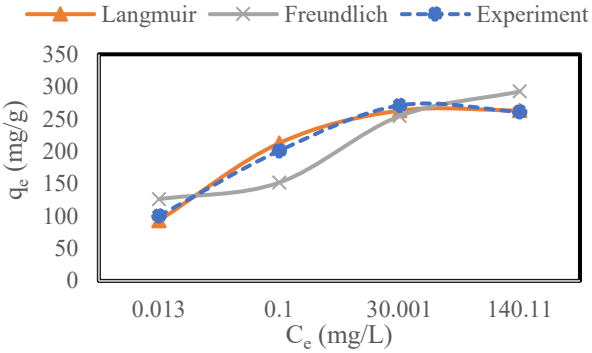

Figure 6. Non-linear plot of adsorption isotherms for adsorption of CAP using CHAC.

Meanwhile, it is apparent from Figure 7(a) that the pseudo first order (PFO) plot does not match the experimental data the most. This finding correlates to the low correlation efficient (R2) values of 0.4989 to 0.7818 at varying concentrations of 100 mg/L to 400 mg/L, respectively. The calculated values fluctuate from starting of the experiment until the 180th min of experiment. In addition, the calculated adsorption capacities, q_{cal} associated with the PFO model imply a very huge difference compared to the adsorption capacities determined from the experiment, q_{exp}. The calculated q_{cal} using PFO model of 100 mg/L gives a value of 10.8547 mg/g, which is much lower than q_{exp} obtained from experimental (q_{exp} = 100.393 mg/g). The difference is correlated to the standard deviation (SD), σ which evidently shows a large variation in the data upon fitting.

Contrarily, the PSO model seems match with data obtained from the experiment better than the PFO model. Based on Figure 7(b), the PSO model fits most of the points accurately, with R_2 values of 0.9998, 0.9998, 0.9954 and 0.9996 for 100 mg/L to 400 mg/L with 100 mg/L interval, respectively. The absolute fitting of PSO model also corresponds to the adsorption capacities, q_{cal} of 102.0408 mg/g, 204.0816 mg/g, 277.7778 mg/g and 270.2703 mg/g at the respective concentrations. This indicates that the adsorption of CAP using CHAC is best explained by the second order reaction, where adsorption process is governed by chemisorption step as suggested by the PSO model. Thus, it can be deduced that the adsorption of CAP using CHAC from this study is based on the second order reaction, with chemisorption as the rate-controlling step as proven by this analysis.

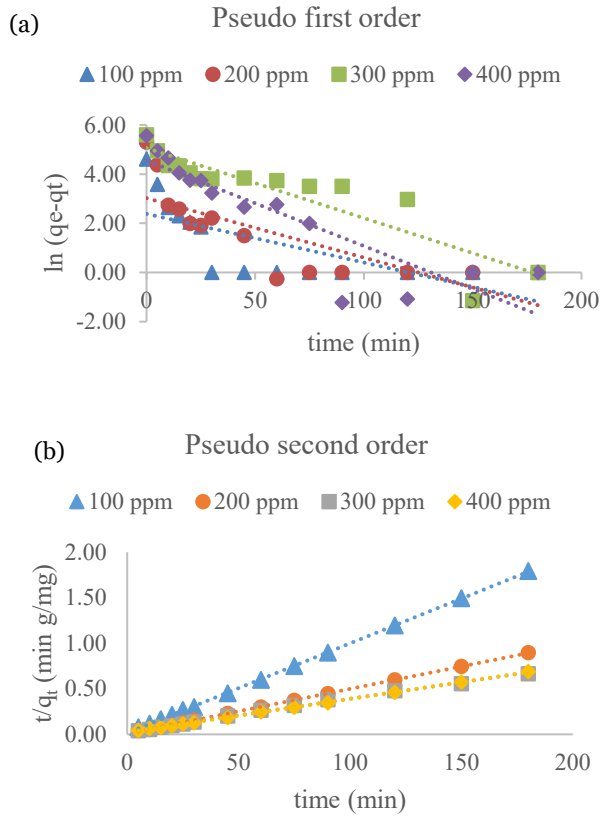

Figure 7. Pseudo first order kinetic model (a) and pseudo second order kinetic model (b).

IV. CONCLUSION

The hydrothermal carbonisation of coconut husk with $ZnCl_2$ activation has been proven to be a good alternative to produce CHAC. Evidently, surface area of CHAC has drastically expanded to 740.7451 m^2/g from 22.9527 m^2/g prior to activation. From SEM analysis, the morphology of CHAC has been enhanced with more visible pores of approximately uniform size on the adsorbent surface. The highest capacity of CHAC adsorption recorded at pH 9 with 99.95% removal. Adsorption isotherm study shows maximum adsorbent capacity, q_{max} of 263.158 mg/g obtained from the Langmuir isotherm model suggesting that the CAP adhere to specific sites on the monolayer surface of CHAC. This results also

show that PSO model is the best (R^2 ranging from 0.9995 to 0.9998 at different CAP concentration) fitting with the experiment data indicating that the adsorption process is based on the second order reaction, with chemisorption as the rate-controlling step.

V. ACKNOWLEDGEMENT

The authors gratefully thanked the School of Chemical Engineering, Universiti Sains Malaysia for the facilities and RUI grant no. 1001/PJKIMIA/8014139 for the opportunities to conduct this work.

VI. REFERENCES

Ahmad, KR, Anwar, SS, Yusup, S, Sham, DS, Inayat, M & Aminu, UH 2022, 'Exploring the potential of coconut shell biomass for charcoal production', Ain Shams Engineering Journal, vol. 13, p. 101499.

Ajala, OA, Akinnawo, SO, Bamisaye, A, Adedipe, DT, Adesina, MO, Okon-Akan, OA, Adebusuyi, TA, Ojedokun, AT, Adegoke, KA & Bello, OS 2023, 'Adsorptive removal of antibiotic pollutants from wastewater using biomass/biochar-based adsorbents', RSC Adv., vol. 13, p. 4678.

Allwar, Ahmad, MN & Mohd, AMN 2008, 'Textural Characteristics of Activated Carbons Prepared from Oil Palm Shells Activated with $ZnCl_2$ and Pyrolysis Under Nitrogen and Carbon Dioxide', Journal of Physical Science, vol. 19, no. 2, pp. 93-104.

Bello, OS, Moshood, MA, Ewetumo, BA & Afolabi, IC 2020, 'Ibuprofen removal using coconut husk activated Biomass', Chemical Data Collections, vol. 29, p. 100533.

Chen, A, Pang, J, Wei, X, Chen, B & Xie, Y 2021, 'Fast one-step preparation of porous carbon with hierarchical oxygen-enriched structure from waste lignin for chloramphenicol removal', Environmental Science Pollution Research, vol. 28, pp. 27398–27410.

Feder, HM, Jr, CO & Maderazo, EG 1981, 'Chloramphenicol: A Review of Its Use in Clinical Practice', Reviews of Infectious Diseases, vol. 3, pp. 479-491.

Foo, KY & Hameed, BH 2012, 'Coconut husk derived activated carbon via microwave induced activation: Effects of activation agents, preparation parameters and adsorption performance', Chemical Engineering Journal, vol. 184, pp. 57-65.

Freundlich, HMF 1906, 'Über die Adsorption in Lösungen. Zeitschrift für Physikalische Chemie', vol. 57, pp. 385-490.

Hammond, KD & Conner, Jr. WC 2013, 'Chapter One - Analysis of Catalyst Surface Structure by Physical Sorption. In: *Advances in Catalysis',* Academic Press, pp. 1-101.

Hien, TT, Vu, NT, Phuong, PTQ, Thien, PH, Thanh, ND & Tuan, PD 2016, 'Optimizing the process of transforming coffee husks into biochar by means of hydrothermal carbonization', Journal of Science and Technology, vol. 54, no. 4B, pp. 138-145.

Idris-Hermann, KT, Raoul, TD, Giscard, D & Gabche, AS 2018, 'Preparation and Characterization of Activated Carbons from Bitter Kola (*Garcinia kola*) Nut Shells by Chemical Activation Method Using H3PO4; KOH and $ZnCl_2$', Chemical Science International Journal, vol. 23, pp. 1-15.

Islam, MA, Ahmed, MJ, Khanday, WA, Asif, M & Hameed, BH 2017, 'Mesoporous activated coconut shell-derived hydrochar prepared via hydrothermal carbonization-NaOH activation for methylene blue adsorption', Journal of Environmental Management, vol. 203, pp. 237-244.

Jain, A, Balasubramanian, R & Srinivasan, MP 2015, 'Tuning hydrochar properties for enhanced mesopore development in activated carbon by hydrothermal carbonization', Microporous and Mesoporous Materials, vol. 203, pp. 178-185.

Kristianto, H, Lavenki, Y & Susanti, RF 2020, 'Synthesis and Characterization of Activated Carbon Derived from *Salacca* Peel Using $ZnCl_2$ Hydrothermal Carbonization and Chemical Activation with Microwave Heating', IOP Publishing Ltd, pp. 012044.

Kowanga, KD, Gatebe, E, Mauti, GO & Mauti, E 2016, 'Kinetic, sorption isotherms, pseudo-first-order model and pseudo-second-order model studies of Cu(II) and Pb(II) using defatted *Moringa oleifera* seed powder', The Journal of Phytopharmacology, vol. 5, no. 2, pp. 71-78.

Li, Y, Li, Y, Zang, H, Chen, L, Meng, Z, Li, H, Ci, L, Du, Q, Wang, D, Wang, C, Li, H & Xia, Y 2020, '$ZnCl_2$-activated carbon from soybean dregs as a high efficiency adsorbent for cationic dye removal: isotherm, kinetic, and thermodynamic studies', Environmental Technology, vol. 41, pp. 2013-2023.

Liew, JH & Hamid, NA 2023, 'Properties of hydrochar produced by hydrothermal carbonization using coconut husk', AIP Conference Proceedings, vol. 2785, no. 1, p. 030004.

Man, HC, Akinbile, CO & Chin, XJ 2015, 'Coconut Husk Adsorbent for the Removal of Methylene Blue Dye from Wastewater', BioResources, vol. 10, no. 2, pp. 2859-2872.

Nakahara, O 1996, 'Reconsideration of theoretical basis of Freundlich adsorption isotherm equation', Soil Science and Plant Nutrition, vol. 42, no. 1, pp. 51-61.

National Centre for Biotechnology Information, 2021.

Sharma, HB, Sarmah, AK & Dubey, B 2020, 'Hydrothermal carbonization of renewable waste biomass for solid biofuel production: A discussion on process mechanism, the influence of process parameters, environmental performance and fuel properties of hydrochar', Renewable and Sustainable Energy Reviews, vol. 123, p. 109761.

Sultana, S, Islam, K, Hasan, MA, Khan, HMJ, Khan, MAR, Deb, A, Al Raihan, M & Rahman, MW 2022, 'Adsorption of crystal violet dye by coconut husk powder: Isotherm, kinetics and thermodynamics perspectives', Environmental Nanotechnology, Monitoring & Management, vol. 17, p. 100651.

Tan, IAW, Ahmad, AL & Hameed, BH 2008, 'Adsorption of basic dye on high-surface-area activated carbon prepared from coconut husk: Equilibrium, kinetic and thermodynamic studies', Journal of Hazardous Materials, vol. 154, no. 1-3, pp. 337-346.

Yay, ASE, Birinci, B, Açıkalın, S & Yay, K 2021, 'Hydrothermal carbonization of olive pomace and determining the environmental impacts of post-process products', Journal of Cleaner Production, vol. 315, p. 128087.

Yu, J, Hou, X, Hu, X, Yuan, H, Wang, J & Chen, C 2019, 'Efficient degradation of chloramphenicol by zero-valent iron microspheres and new insights in mechanisms', Applied Catalysis B: Environmental, vol. 256, p. 117876.

Yun, TZ 2019, 'Agriculture: A coconut revival', retrieve from <www.theedgemarkets.com/article/agriculture-coconut-revival>.

Yusop, MFM, Ahmad, MA, Rosli, NA & Abd, Manaf, ME 2021, 'Adsorption of cationic methylene blue dye using microwave-assisted activated carbon derived from acacia wood: Optimization and batch studies', Arabian Journal of Chemistry, vol. 14, no. 6, p. 103122.

Zhang, T, Yang, Y, Li, X, Jiang, Y, Fan, X, Du, P, Li, H, Wang, N & Zhou, Z 2021 'Adsorption characteristics of chloramphenicol onto powdered activated carbon and its desorption performance by ultrasound', Environmental Technology, vol. 42, no. 4, pp. 571-583.